New insight into the electronic structure of iron(IV)-oxo porphyrin compound I. A quantum chemical topological analysis

4 **AUTHORS**, INCLUDING:

Ignacio Viciano
Universitat Jaume I
3 PUBLICATIONS   **6** CITATIONS

Available from: Ignacio Viciano
Retrieved on: 25 January 2016

New Insight into the Electronic Structure of Iron(IV)-oxo Porphyrin Compound I. A Quantum Chemical Topological Analysis

Ignacio Viciano, Slawomir Berski, Sergio Martí,* and Juan Andrés

The electronic structure of iron-oxo porphyrin π-cation radical complex $Por^{.+}Fe^{IV}=O$ (S—H) has been studied for doublet and quartet electronic states by means of two methods of the quantum chemical topology analysis: electron localization function (ELF) $\eta(r)$ and electron density $\rho(r)$. The formation of this complex leads to essential perturbation of the topological structure of the carbon–carbon bonds in porphyrin moiety. The double C=C bonds in the pyrrole anion subunits, represented by pair of bonding disynaptic basins $V_{i=1,2}(C,C)$ in isolated porphyrin, are replaced by single attractor $V(C,C)_{i=1-20}$ after complexation with the Fe cation. The iron–nitrogen bonds are covalent dative bonds, N→Fe, described by the disynaptic bonding basins $V(Fe,N)_{i=1-4}$, where electron density is almost formed by the lone pairs of the N atoms. The nature of the iron–oxygen bond predicted by the ELF topological analysis, shows a main contribution of the electrostatic interaction, $Fe^{\delta+}\cdots O^{\delta-}$, as long as no attractors between the C(Fe) and C(O) core basins were found, although there are common surfaces between the iron and oxygen basines and coupling between iron and oxygen lone pairs, that could be interpreted as a charge-shift bond. The Fe—S bond, characterized by the disynaptic bonding basin $V(Fe,S)$, is partially a dative bond with the lone pair donated from sulfur atom. The change of electronic state from the doublet ($M = 2$) to quartet ($M = 4$) leads to reorganization of spin polarization, which is observed only for the porphyrin skeleton (−0.43e to 0.50e) and S—H bond (−0.55e to 0.52e). © 2012 Wiley Periodicals, Inc.

Introduction

Cytochrome P450 enzymes is a superfamily of hemoproteins that plays an important role in some biological processes in several bioorganisms such as plants, mammalian, fungi, archaea, bacteria, or protists.[1,2] This superfamily is composed by a large number of isoforms which can metabolize a wide variety of endogenous as well as exogenous substrates.[3]

The most important catalyzed reaction by the cytochrome P450 enzymes is the monooxygenation of organic substrates:

$$RH + O_2 + 2H^+ + 2e^- \rightarrow ROH + H_2O$$
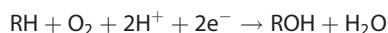
in which an oxygen atom is inserted into the unactivated C—H bond of an organic substrate via oxygen activation process. In fact, this is the reason why Cytochrome P450 is also called monooxygenase and it is well known as one of the most versatile oxidant in the nature.[3]

During the catalytic cycle of this enzyme, an iron-(IV) oxo-porphyrin π-cation radical specie ($Por^{.+}$ $Fe^{IV}=O(S\text{-}Cys)$) also known as Compound I (Cpd I) is formed.[4] This Cpd I (Scheme 1) is an elusive specie in the catalytic cycle of the cytochrome P450 and is the key step in the oxidation of substrates.[5] It is based on a protoporphyrin-IX prosthetic group with a central iron atom linked to two axial ligands: the first one is a cysteine amino acid named as proximal axial ligand and the second one is an oxo anion named distal ligand, which forms a ferryl $Fe^{IV}=O$ moiety. Cpd I is also formed in the catalytic cycle of other proteins, such as peroxidase or catalase, whose proximal axial ligands are the histidine and tyrosine amino acids, respec-
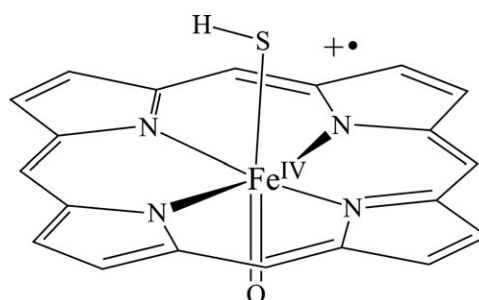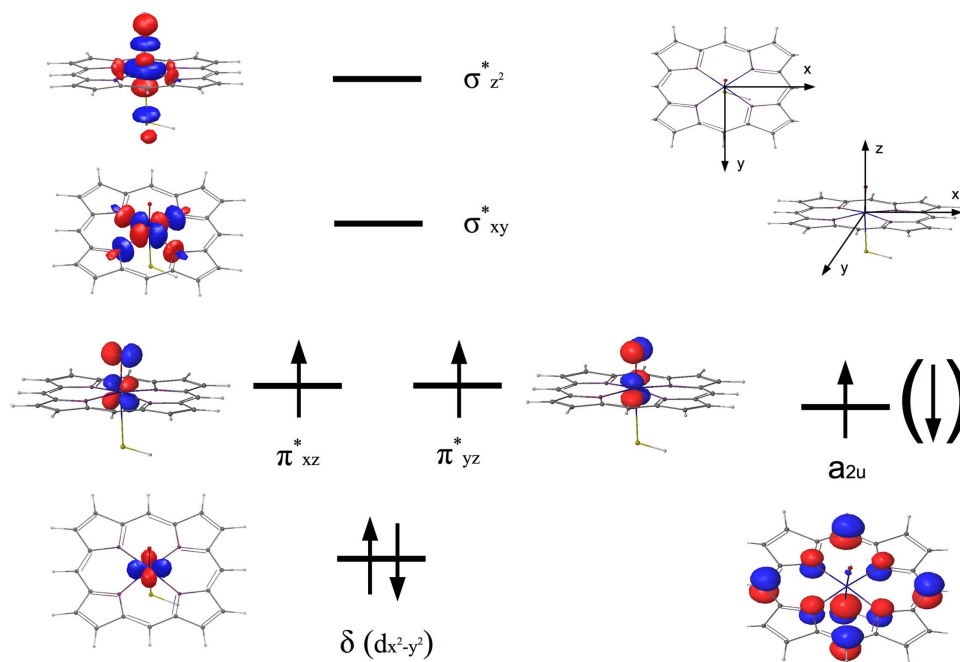

Scheme 1. Lewis structure of Compound I.

tively. As a result, the elusiveness of Cpd I and due to the high reactivity, which makes it very difficult to detect, other alternative oxidant species such as Compound 0[6] ($Por—Fe^{III}—OOH^-$, Cpd 0), Compound II[7] ($Por—Fe^{IV}=O$, Cpd II) as well as perferryl species[8,9] ($Por—Fe^V=O$) have been suggested that could be the reactive intermediates in the oxidation of the substrates by the

[a] I. Viciano, S. Martí, J. Andrés
Departamento de Química-Física y Analítica, Universitat Jaume I, 12071, Castelló, Spain
[b] S. Berski
Faculty of Chemistry, University of Wroclaw, F. Joliot-Curie 14, 50-383 Wroclaw, Poland
E-mail: smarti@uji.es

$\sigma^*_{z^2}$

σ^*_{xy}

π^*_{xz} π^*_{yz}

a_{2u}

$\delta\ (d_{x^2-y^2})$

Scheme 2. Molecular orbitals diagram of doublet and quartet spin states for Compound I. [Color figure can be viewed in the online issue, which is available at wileyonlinelibrary.com.]

the porphyrin and the sulfur atom of the axial ligand. As a result of the dual character in the spin state, Shaik et al.[19] proposed that a two state reactivity (TSR) mechanism is operative along the most common reactions of Cpd I of Cytochrome P450, which are the hydroxylation of alkanes and the epoxidation of alkenes.

Since the end of the 1990s with the pioneer work of Loew,[20–23] several theoretical studies have been carried out to calculate the electronic structure and spectra of the Cpd I, both in gas phase and in the enzyme environment. Very recently, Shaik et al.[13] have published a review on the theoretical works devoted to study the structure, reactivity, and selectivity on different P450 enzymes. In this review, the electronic structure of Cpd I is analyzed by means of different levels of theory, such as the orbital approach using density functional theory (DFT) calculations, multireference *ab initio* methods, as well as the valence bond theory.

The relationship between charge density topology and physical/chemical properties can be understood from the Hohenberg–Kohn theorem, which asserts that a system's ground-state properties are a consequence of its charge density, a scalar field denoted as $\rho(r)$.[24] Indeed, Bader[25] noted that the essence of a molecule's structure must be contained within the topology of $\rho(r)$. Thus, the quantum theory of atoms in molecules (QT AIM or in short AIM) developed by Bader et al.,[25] is a method based on the topology of the electron density $\rho(r)$, a physical observable that can be determined from electronic structure theory calculations or experimentally, and its Laplacian, $\nabla^2\rho(r)$, and it has enjoyed great success as a tool to analyze and rationalize chemical bonding in molecules. In addition, real-space partitioning of the molecular space may also be achieved by using functions of the electronic density and/or its derivatives. Conversely, the electron localization function (ELF), $\eta(r)$, proposed by Becke and Edgecombe[26] in 1990, allows for the mapping of electron pair probability in multielectron systems based on the electron density. The topological analysis of $\eta(r)$, proposed in 1994 by Silvi and Savin,[27–29] permits to perform a quantitative analysis of the three-dimensional function, providing useful information on the electronic structure. Both scalar fields can be considered within the quantum chemical topology framework[30] as proposed by Popelier et al.,[30,31] to describe accurately chemical concepts of atoms, bonding, and molecular structure.

Topological analysis of the $\eta(r)$ function has been already used to study iron porphyrins. Novozhilova et al.[32] and Xu

cytochrome P450. However, very recently, Rittle and Green prepared Cpd I in a high concentration on CYP119 P450 cytochrome, being able to confirm the ability of this specie to produce the oxidation of unactivated C—H bonds,[10] confirming the important role of the Cpd I as active oxidant in P450 enzymes.

The Cpd I is a radical and it is well known that there are two low-lying spin states (doublet and quartet), due to the ferromagnetic/antiferromagnetic coupling between a triplet formed by the Fe=O moiety and a doublet formed by an odd electron, which has a porphyrinic nature and is delocalized toward the sulfur atom of the ligand. The accepted electronic structure of this compound (Scheme 2) consists in a π-antibonding triplet formed by the ferryl Fe^{IV}=O moiety (π^*_{xz} and π^*_{yz} orbitals) and a π character a_{2u} radical orbital which can couple ferromagnetically to provide a high-spin (HS) state with $S = 3/2$ or antiferromagnetically to provide a low-spin (LS) state with $S = 1/2$, being both states almost degenerated.[11–13] The role of the axial ligand in the electronic structure of Cytochrome P450 Cpd I has been studied by several researchers using different kinds of thiolate models: SH, SMe, SCys, or Cysteinate, concluding that the ground state of this compound depends on the nature of the thiolate used due to the donor character of the sulfur of each model and the interaction of that atom with the environment.[13] In fact, in the experiments where the SMe[14] and S-cys[15] were chosen as axial ligands, it was observed that the spin density of the unpaired radical resided mainly in a lone-pair of the sulfur atom of the ligand, being scarce the contribution of the porphyrin ring. Conversely, in the cases where the SH and Cysteinate models (which has internal hydrogen bonding) were chosen,[16–18] it was observed that the a_{2u} porphyrin orbital is singly occupied being the spin density distributed between

et al.[33] illustrated "ferrous" {FeNO}^{7}-like electron pair localization on a nitrosyl N-atom in a "ferric" {FeNO}^{6} porphyrin. In the Fe–NO region, the disynaptic bonding basin V(Fe,N) has been observed which corresponds to the Fe—N bond and the V(N,O) disynaptic bonding basin characterizing nitrogen–oxygen bond. Furthermore, this methodology has been applied to study the nature of metal-oxygen bond in other systems,[34,35] which feature a high ionic character in this kind of bonds, due to the lack of disynaptic basins between both atom cores.

In this article we investigate, for the first time, the electronic structure of Cpd I by using the topology of both ELF, $\eta(r)$, and electron density, $\rho(r)$. This allows us to broaden the spectrum of information known about the nature of this compound with so much biological interest, providing new insight into the nature of the bonds and the electronic distributions of its two most characteristic spin states: doublet and quartet.

Computational Details

Full geometry optimizations of the Por$^{\cdot+}$ Fe^{IV}=O(S—H) complex in doublet and quartet electronic states have been performed using the unrestricted formalism with the UB3LYP density functional as well as the LACVP* basis set[36] (consisting of the combination of the 6-31G(d) basis for all the atoms except for the iron one, which was represented by the LANL2DZ effective core potential). In addition, single-point energies of the resulting structures have been carried out at the UB3LYP/6-31G(d) level to obtain an accurate wave functions, avoiding the use of pseudopotentials on the iron atom. Conversely, geometrical structures of isolated pyrrole, pyrrole anion, and porphyrin ring have been optimized at the B3LYP/6-31G(d) level. With the aim of obtaining a more accurate description of porphyrin, the geometry optimization and topological analysis of $\eta(r)$ have been repeated at B3LYP/6-311++G(d,p) level. The minima on the potential energy surface have been confirmed by nonimaginary vibrational frequencies. All the calculations were performed using the Gaussian 03 program.[37]

The ELF function [$\eta(r)$] provides regions of the space, where the probability of finding an electron pair in the molecular space is high. The topological analysis of this function yields basins of attractors corresponding to atomic cores, bonds, and lone pairs. The atomic cores coincide with the atomic nuclei and are labeled as C(A), being A the atomic symbol of the element. The concept of *synapticity*, introduced by Silvi et al.[27,38] allows the classification of η-localization basins in the $\eta(r)$ domain. In this way, it is possible to find monosynaptic basins, labeled as V(A), which correspond to lone pairs of the Lewis model, as well as disynaptic basins labeled as V(X,Y) which correspond with the η-localization basins with common surfaces between two C(X) and C(Y) core basins. Conversely, trisynaptic basins labeled as V(X,Y,Z) correspond to the three-center bonds, and so on. The integration of the electron density over the different basins yields to the basin population, $\overline{N}$, allowing the quantification of possible charge transfer phenomena. In the present work, the topological analysis of the ELF $\eta(r)$ and electron density $\rho(r)$ has been carried out using Dgrid-4.5 program[39] over a rectangular parallelepiped grid with a step of 0.05 bohr. Graphical representations have been generated by means of the

Jmol,[40] visual molecular dynamics (VMD),[41] and UCSF Chimera package[42] programs.

Results and Discussion

The optimized geometry of the Cpd I model compound, the isolated porphyrin, the isolated pyrrole, and the pyrrole anion are depicted in Figure 1. As can be observed the C2—C3 and C4—C5 distances are shorter than the C1—C2 lengths in both the Cpd I and the isolated porphyrin, which means a larger bond order in the former bonds, thus exhibiting a large amount of double bond character. However, this behavior differs from the one observed in both the isolated pyrrole and the pyrrole anion, where the C2—C3 bond length is larger than the C1—C2 or C3—C4 ones (see Figs. 1c and 1d). Since the porphyrin ring can be seen as four pyrrole rings connected by methine bridges (=CH—), the splitting of this large macrocycle into its subunits leads to changes in the bond lengths and thus in the degree of delocalization. With respect to the C—N distances, the values obtained for Cpd I indicate a partial double bond character as well, similar to those found in the isolated porphyrin, the isolated pyrrole, and in the pyrrol anion ring.

Furthermore, all the values for the Fe—N distances of Cpd I ($\sim$2.02 Å) point out the fact that Fe—N interactions should be of the same nature. In Figure 1b, the Fe—O and Fe—S distances as well as the S—Fe—O angle are also depicted. The Fe—O distance in both spin states is around 1.63 Å, which is in good agreement with experimental x-ray absorption spectroscopy data found in the literature for Cpd I (1.65 Å).[43] However, the Fe—S bond exhibits a larger distance (2.60 Å) than the found experimentally (2.48 Å using EXAFS spectroscopy[43]). Nevertheless, this result is comparable to other theoretical studies, which also makes use of the SH axial ligand and DFT methodology, indicating that the strong interactions between the thiolate and oxo ligands provokes a large value for the Fe—S bond.[5,14,18] Finally, the value of the S—Fe—O angle shows an almost colinear distribution of both the proximal SH and the distal Oxo ligands ($\sim$171° in average).

The electronic structure of Cpd I, in both doublet and quartet electronic states, is characterized by 76 local maxima (attractors) localized for the field of ELF $\eta(r)$. The spatial localization of all attractors is presented at Figure 2. The core electron density is characterized by a total of 27 core attractors C(Fe), C(S), C(O), C(N)$_{i=1-4}$, and C(C)$_{i=1-20}$ which coincide with positions of atomic nuclei. Conversely, in the valence shell, the electrons are associated with three monosynaptic nonbonding basins (attractors): V(S) and V$_{i=1,2}$(O) corresponding to the lone pairs of the sulfur and oxygen atoms, respectively. Furthermore, a total of 33 valence disynaptic bonding attractors can be observed: V(C,C)$_{i=1-20}$, V(C,N)$_{i=1-8}$, V(Fe,S), and V(Fe,N)$_{i=1-4}$, corresponding to the C—C, C—N$_{i=1-8}$, Fe—S, Fe—N$_{i=1-4}$ chemical bonds, respectively. The C—H and S—H bonds are reflected by 12 protonated disynaptic attractors V(H,C)$_{i=1-12}$ and one V(H,S) attractor. According to interpretation proposed by Silvi and Savin,[27] the localization of the valence bonding attractors V(A,B) yields proof that considered A—B bonds are of the covalent type.

It is worth noting, that the same number and type of attractors are localized for the Cpd I system in both the doublet
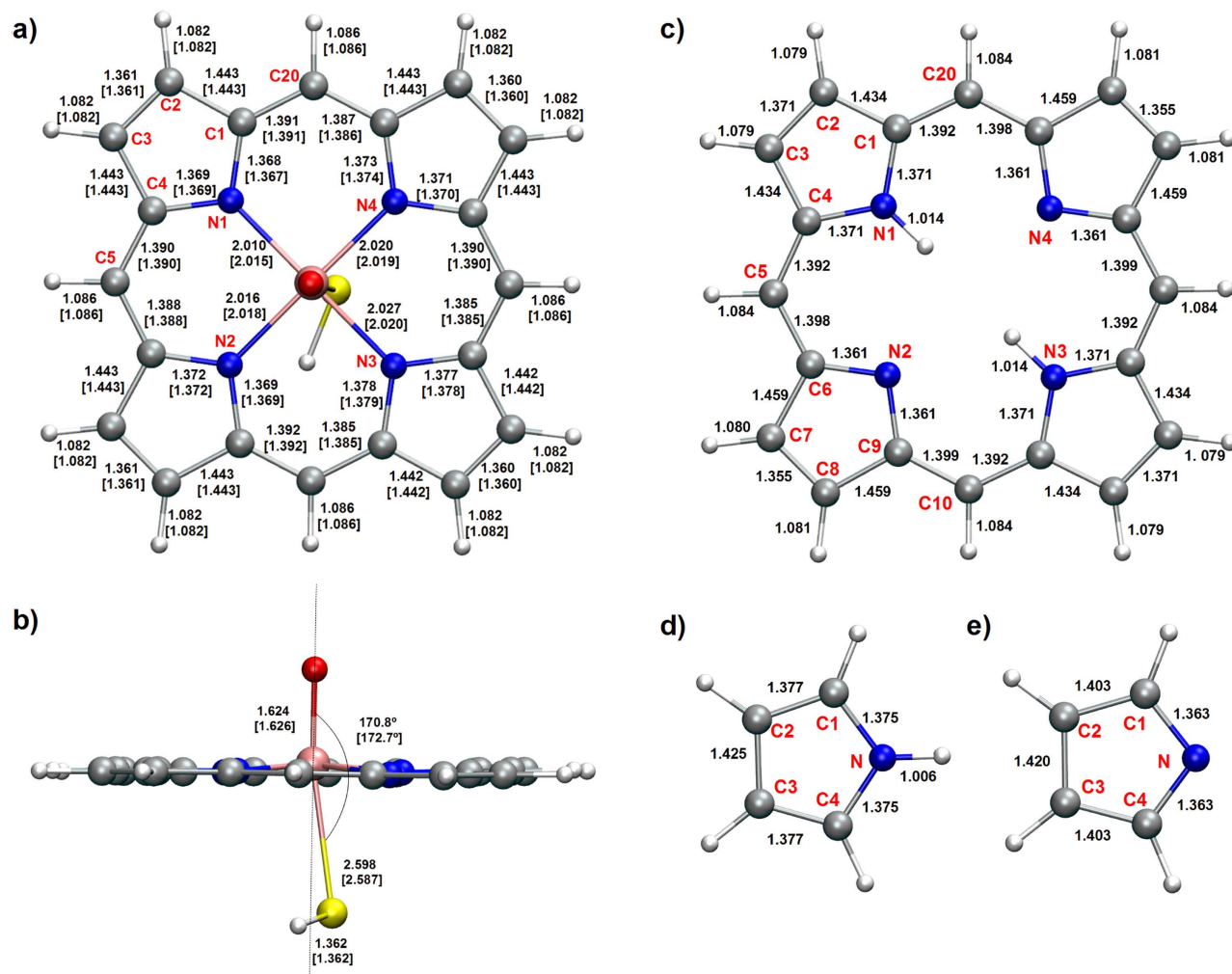
Figure 1. Geometrical parameters for: a) and b) the optimized Cpd I, in doublet and [quartet] spin states, c) the porphyrin ring, d) the pyrrole molecule, and e) the pyrrole anion. The distances are expressed in angstroms and angles in degrees. [Color figure can be viewed in the online issue, which is available at wileyonlinelibrary.com.]

and quartet electronic states. The unique difference is the slightly different spatial orientation of the $V_{i=1,2}(O)$ attractors regarding the Fe—N bonds and the porphyrin plane which can be associated with occupation of different orbitals in both electronic states as shown in Figure 2.

The core attractors C(Fe), C(N)$_{i=1-4}$, C(C)$_{i=1-20}$ and the valence attractors V(H,C)$_{i=1-12}$, V(C,C)$_{i=1-20}$, V(C,N)$_{i=1-8}$, V(Fe,N)$_{i=1-4}$ reflect the electronic structure of the iron-porphyrin complex: the planar geometry of porphyrin is associated with the aromatic character originated by the conjugation of the double C=C and C=N bonds. As a matter of fact, all attractors are observed lying approximately within the porphyrin plane. Finally, the lack of the $V_{i=1,2}$(C,C) or $V_{i=1,2}$(C,N) attractors above and below the macrocycle ring plane, resembles the topology of $\eta(r)$ observed in other molecules with large delocalization of the electron density, such as for instance benzene[44] or pyridine.[45] The porphyrin ring in Cpd I is built from four pyrrole subunits, where the hydrogen atoms from two N—H bonds (in parent porphyrin) have been removed. Thus, the differences between the electronic structure of Cpd I and its subunits may be obtained from the comparison with

the electronic structure of isolated pyrrole (C_4H_4NH), pyrrole anion ($[C_4H_4N]^-$), and porphyrin ring. The core and valence attractors localized in the three molecules are shown in Figure 3, whereas the basin populations are presented in Table 1.

The topology of the $\eta(r)$ function for the pyrrole anion—considering a number of attractors and their synapticity[38,46]—is the same as observed for the Cpd I. In both C_4H_4NH and $[C_4H_4N]^-$ molecules the valence attractors, corresponding to delocalized C=C and C—N bonds, are found in the molecular plane. The main difference is found for regions where nitrogen lone pairs are expected. The nonbonding electron density of the N atom in C_4H_4NH is reflected by two nonbonding $V_{i=1,2}$(N) attractors localized below and above molecular plane, meanwhile in the $[C_4H_4N]^-$ anion only single nonbonding attractor V(N) in the plane is localized.

The basin population of V(N) increases from 1.08e for C_4H_4NH to 3.03e for $[C_4H_4N]^-$, value which is very similar to those calculated for the V(Fe,N)$_{i=1-4}$ basins in Cpd I (3.04e). This fact supports the observation that the V(Fe,N)$_{i=1-4}$ basin consists mainly of electrons from the lone pair of the nitrogen atom. However, the distance between the V(Fe,N)$_{i=1-4}$ and
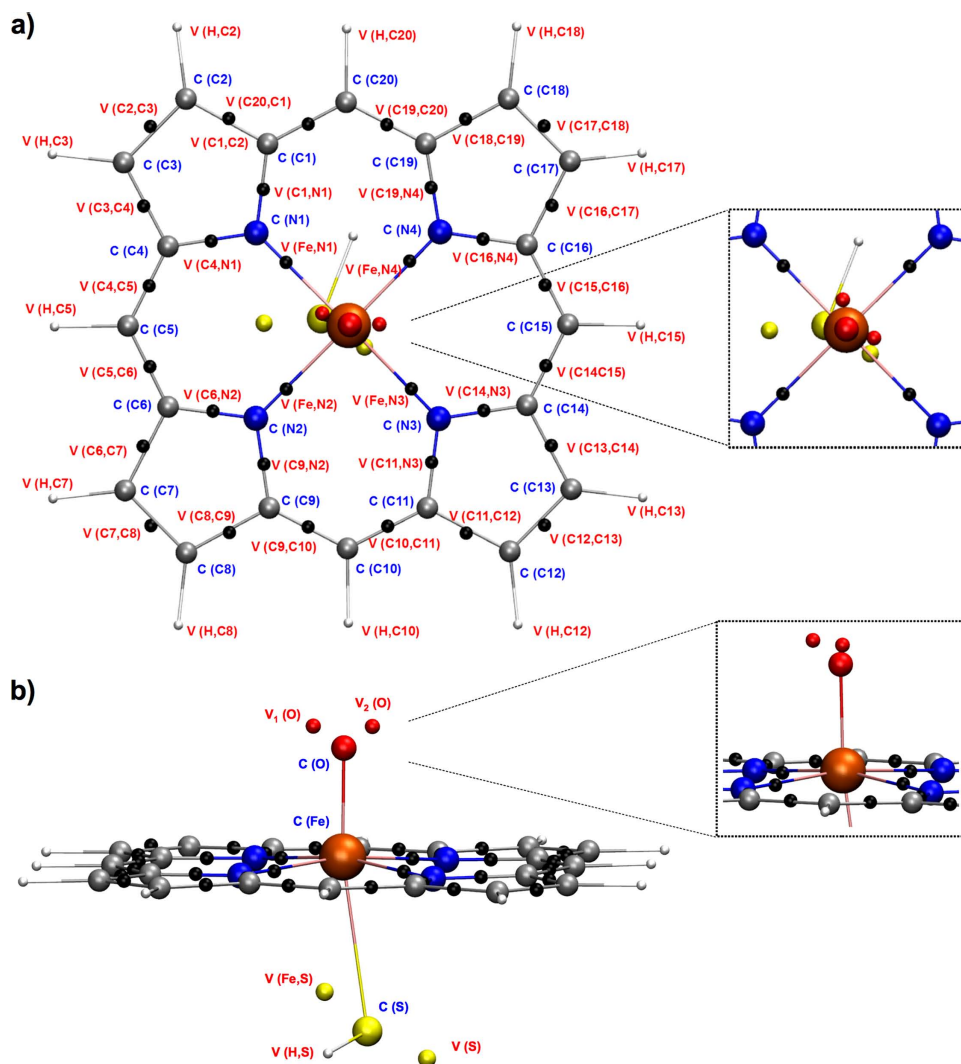
Figure 2. Local maxima attractors localized for the field of electron localization function $\eta(r)$ in Cpd I. Core attractors are depicted in blue and valence attractors in red. a) Attractors in porphyrin ring in doublet state. b) Attractors localized for iron axial ligands in double state. Small boxes represent quartet state. [Color figure can be viewed in the online issue, which is available at wileyonlinelibrary.com.]

$C(N)_{i=1-4}$ attractors in Cpd I (0.64–0.66 Å) are shorter than between the V(N) and C(N) attractors in the pyrrole anion (0.73 Å). This fact may be explained as result of a Pauli repulsion between electrons "contained" in the C(Fe) and $V(Fe,N)_{i=1-4}$ basins and the corresponding "compression" of the electron density in this region.

The electronic structure of isolated Por obtained using topological analysis of $\eta(r)$ is shown in Figure 3c. An interesting topological feature is found for the C2—C3 and C12—C13 bonds of the pyrrole anion fragments, where pairs of the bonding disynaptic attractors $V_{i=1,2}(C,C)$ are localized. The same topological feature has been achieved at B3LYP/6-311++G(d,p) computational level. It is worth emphasizing that in isolated pyrrole anion only a single disynaptic attractor is found (Fig. 3b). The presence of two bonding $V_1(C,C)$ and $V_2(C,C)$ attractors suggests that these carbon–carbon bonds have double bond character, and the degree of electron delocalization is smaller than for other C—C bonds. As showed by

Silvi et al.,[27] the localization of two $V_{i=1,2}(C,C)$ attractors is typical for compounds with formal C=C bonds and has been described using the synapticity concept for the first time in ethylene, propene, and trans-butadiene.[46] The double bond character is also supported by a comparison of the bond length in the porphyrin (1.36 Å), pyrrole (1.43 Å), and pyrrole anion (1.42 Å), which shows that the C=C bond in the porphyrin is the shortest one. Since all C—C bonds in Cpd I are represented by single $V(C,C)_{i=1-20}$ attractors, the Por$^{\cdot+}$ Fe^{IV}=O(S—H) complex formation would result in an increase of the electron density delocalization over the molecule. Thus, a number of resonance hybrids, based on Lewis formula, have to be considered. The bond order for delocalized bonds should be between 1 and 2, and the values of the basin populations support this expectation, being in the range 2.39e–3.29e, and topological bond orders between 1.2 and 1.6, in both electronic states (see Supporting Information Tables S1 and S2).

Three groups of carbon–carbon bonds with very similar values of the basin population (Fig. 4) are found. These values may be associated with the localized nature of the bonds. Furthermore, the topological analysis of ELF shows that the perturbation exerted by the HS ligand in the Cpd I, which lacks of the C4 symmetry axis present in the porphyrin ring, is quite small providing almost the same basin populations in each of the four Cpd I fragments.

The largest values of $\overline{N}$, (3.30e) are obtained for the C2,C3; C7,C8; C12,C13; and C17,C18 pairs of atoms (I group) in the pyrrole subunits. In fact, the resonance hybrids which are usually proposed to illustrate the delocalized character of the porphyrin bonds suggest a dominant contribution of the C=C bonding. It is worth noting that these bonds have a clear double bond character in the isolated porphyrin, as long as they are represented by two $V_{i=1,2}(C,C)$ attractors. Conversely, the carbon–carbon bonds of the four methine fragments are slightly less populated, with basin populations in the range 2.88e–3.01e (II group). As result, the contribution of resonance
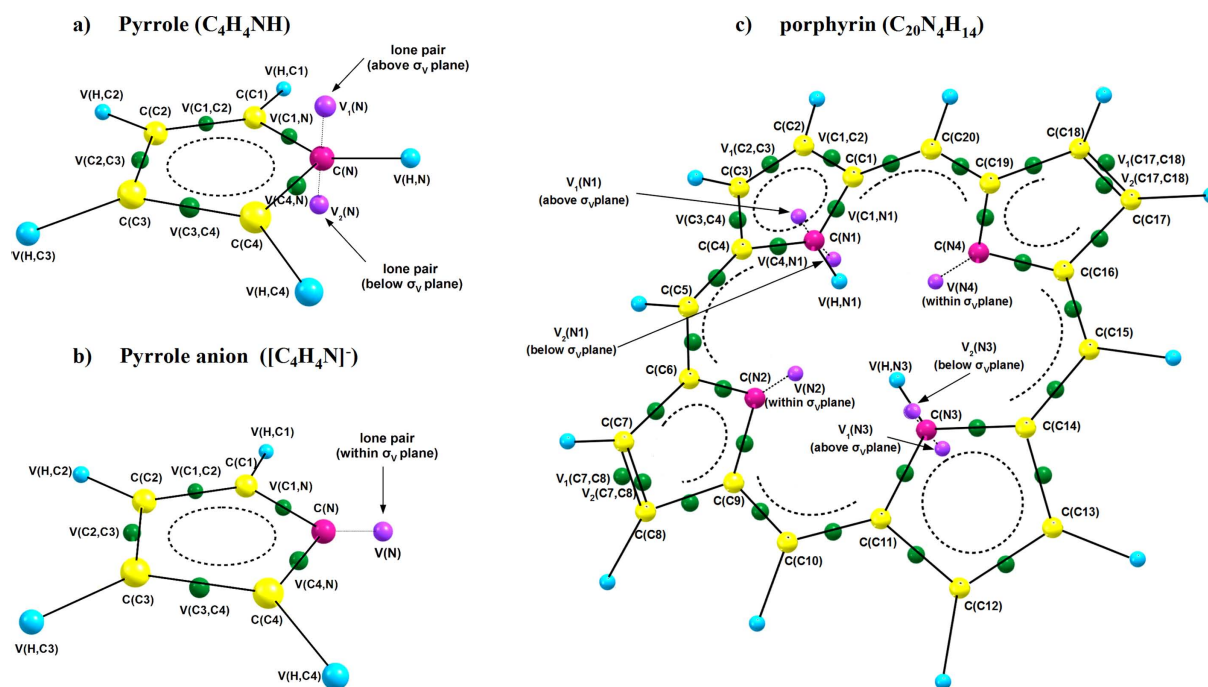
Figure 3. Core and valence attractors localized for pyrrole a), pyrrole anion b), and porphyrin ring c). [Color figure can be viewed in the online issue, which is available at wileyonlinelibrary.com.]

hybrids with double C=C bonds is smaller than postulated for I group. The smallest values of $\overline{N}$ are found for the carbon–carbon bonds in the pyrrole subunits (III group) connecting the group I bonds with the methine "bridges" (=CH—). Their basin populations are approximately 2.39e, values that can be interpreted in terms of the predominant single C—C character. In the same way, those carbon–nitrogen bonds with the smallest basin populations, equal to 2.15e–2.17e, may be characterized as single type C—N bonds. In spite of the essential contribution of the C=N double bond character suggested by the resonance hybrids, the valence electrons are "concentrated" in the disynaptic V(Fe,N)$_{i=1-4}$ of the Cpd I, equivalent to the pyrrole anion V(N) basins, being their value equal to 3.04e in average, which is much larger than the 2e formal value. This fact can be explained analyzing the covariance matrix of the ELF function. In this case, we observe a large cross term in average of the localization

indexes among the V(Fe,N)$_{i=1-4}$ and the corresponding V(C,N)$_{i=1-8}$ (0.36e each, see Supporting Information Table S3). This would mean that the porphyrin ring would be donating electrons to the Fe—N dative bonds.

The presence of these four V(Fe,N)$_{i=1-4}$ basins localized between Fe and four N atoms (see Figs. 2 and 5) may be interpreted as covalent bonds. Topographical analysis of $\eta(r)$ function (2D map, Fig. 5), performed at the molecular plane of Cpd I ($M = 2$) shows that the valence domains observed between the iron and nitrogen core domains are well separated, and the values of $\eta(r)$ function in the Fe$\cdots$N$_{i=1-4}$ regions approach to zero (blue color at Fig. 5). Besides, the degree of electron localization in those regions is below 0.5e, the value corresponding to the free electron gas. Furthermore, the observed separation between 2D-domains indicates that the region of the N lone pair should be associated with a monosynaptic nonbonding basin V(N)$_{i=1-4}$ and interpreted as a lone pair. In fact, a lack of a bonding disynaptic basin implies that the nature of the iron–nitrogen bond is governed by electrostatic interactions, Fe$^{\delta+}\cdots$N$^{\delta-}$, and is not originated in a covalent bonding. However, a 2D map of the $\eta(r)$ function does not clearly shows the localization basins but only a distribution of the $\eta(r)$ values. Therefore, a more accurate description must be performed by means of localization basins: the four nitrogen cores C(N)$_{i=1-4}$, the iron core C(Fe), and the valence basins localized between the Fe and N cores, as

Table 1. Basin populations of the pyrrole C_4H_4NH, pyrrole anion $[C_4H_4N]^-$, porphyrin and pyrrole fragment (C_4H_2N) in Cpd I ($M = 2, 4$); as a result of the topological analysis of electron density $\rho(r)$ and electron localization function $\eta(r)$.

Basin[a]/molecule	C_4H_4NH	$[C_4H_4N]^-$	Porphyrin	Cpd I ($M = 2$)	Cpd I ($M = 4$)
C(N)	2.11e	2.11e	2.11e	2.13e	2.14e
V$_{i=1,2}$(N)	0.54e/0.54e[b]	3.03e[c]	0.53e[b]/3.04e[c]	3.04e[d]	3.03e[d]
r[V$_{i=1,2}$(N)$\cdots$C(N)]	0.65 Å/0.65 Å[e]	0.73 Å[e]	0.65 Å/0.72 Å[e]	0.65 Å[f]	0.64 Å[f]
V(C1,C2);V(C3,C4)	3.30e/3.30e	3.34e/3.34e	2.38e/2.51e	2.39e	2.39e
V(C2,C3)	2.54e	2.65e	3.11e/1.61e	3.30e	3.29e
V(C1,N1); V(C4,N1)	2.18e/2.16e	2.18e/2.15e	2.23e/2.19e	2.16e	2.16e

[a] Numbering of atoms and basins according to Figures 2 and 3. [b] Nonbonding basin V(N) localized in both above and below the molecular plane. [c] Single nonbonding basin V(N) localized in the molecular plane. [d] Bonding disynaptic basin V(Fe,N). [e] Distance between the core attractor of nitrogen C(N) and nonbonding monosynaptic attractor V$_i$(N). [f] Distance between the core attractor of nitrogen C(N) and bonding disynaptic attractor V(Fe,N).

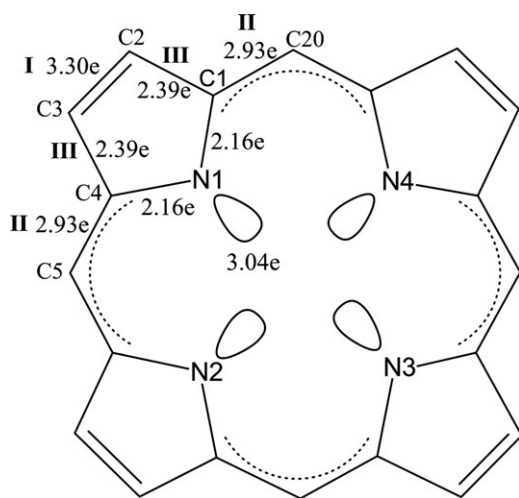**Figure 4.** ELF population analysis for Cpd I porphyrin ring. The different carbon–carbon bond groups (**I**, **II**, and **III**), depending on their population values, are also depicted.

presented in Figure 6. Certainly, each valence basin between N and Fe belongs to a disynaptic $V(Fe,N)_{i=1-4}$ type, as long as it has a common surface with both the $C(N)_{i=1-4}$ and C(Fe) core basins (see Fig. 6c). Thus, the analysis of the synaptic order implies that the iron–nitrogen bonding belongs to the covalent-dative type, as long as the distribution of ELF values shows that the electron density of the bond is mainly formed by the nitrogen lone pair.

A very similar topological structure is observed for the localization basin associated with the valence attractor localized between the C(Fe) and C(S) cores (see Fig. 5). The 2D representation of $\eta(r)$ presented at Figure 5b shows that the domain corresponding to the Fe—S bonding is well isolated from the iron core domain. Most probably it is almost entirely formed by the nonbonding electron density of the sulfur. However, its localization basin has a common surface with C(Fe) core basin (Fig. 6b); and therefore, this valence basin has bonding nature also being disynaptic V(Fe,S), and the covariance matrix of the ELF shows a localization index of 0.45e for the V(S) and 0.25e for the V(H,S). Thus, the sulfur–iron bond, similarly to iron–nitrogen one, has a topological feature of covalent dative character.

Additional information on the nature of the sulfur–iron interaction can be obtained from the comparison with simple molecules (H_2S, HS anion, and HS radical), containing sulfhydryl group. The results of topological analysis of the $\eta(r)$ and $\rho(r)$ functions, performed for B3LYP/6-31G(d) optimized geometrical structures, are shown in Table 2 and Supporting Information Figure S4. In the $[HS]^-$ and $[HS]^.$ molecules, the lone pairs of sulfur are represented by single nonbonding basin V(S) and such topology is similar to that observed for Cpd I. The total basin population of the Fe—S bond and V(S) valence basins, $N[V(Fe,S) + V(S)]$, in the complex is 5.43e for both $M = 2$ and $M = 4$, respectively, which is smaller than the computed for the $[HS]^-$ anion (6.12e) but slightly larger than for the HS radical (5.17e). The population of the H—S bond in Cpd I (1.84e) is similar to the H_2S, $[HS]^-$ and $[HS]^.$ molecules. Thus, the H—S bond may be considered as a single bond from a topological

point of view. Anyway, the most interesting finding is obtained when comparing the positions of the V(Fe,S) and V(S) point attractors in Cpd I and in the $[HS]^-$, $[HS]^.$, H_2S molecules. The distance between the C(S) and V(Fe,S) attractors is shorter than between the C(S) and $V_i(S)$ attractors in H_2S, $[HS]^-$ and $[HS]^.$. This implies that the dysynaptic V(Fe,S) basin does not seem to be a standard Fe—S covalent bond, but rather a V(S) basin lone pair. This result confirms the concept of dative S → Fe bond. In addition, the effect of the lone pair "compression" is very similar to that one observed for the N atoms. The same kind of conclusion can be derived from the analysis of the localizations basins, which shows the presence of common surfaces among the dysynaptic V(Fe,S) and the C(Fe) and C(S) cores (see Fig. 6b).

The oxygen atom, formally bound to iron atom by the double Fe=O bond is described by the core C(O) attractor and two monosynaptic nonbonding attractors $V_1(O)$ and $V_2(O)$. These last two attractors reflect the nonbonding electron density of the oxygen, which according to the symmetry of the complex is represented by two local maxima. Such topology of $\eta(r)$ stays in agreement with the Lewis structure (see
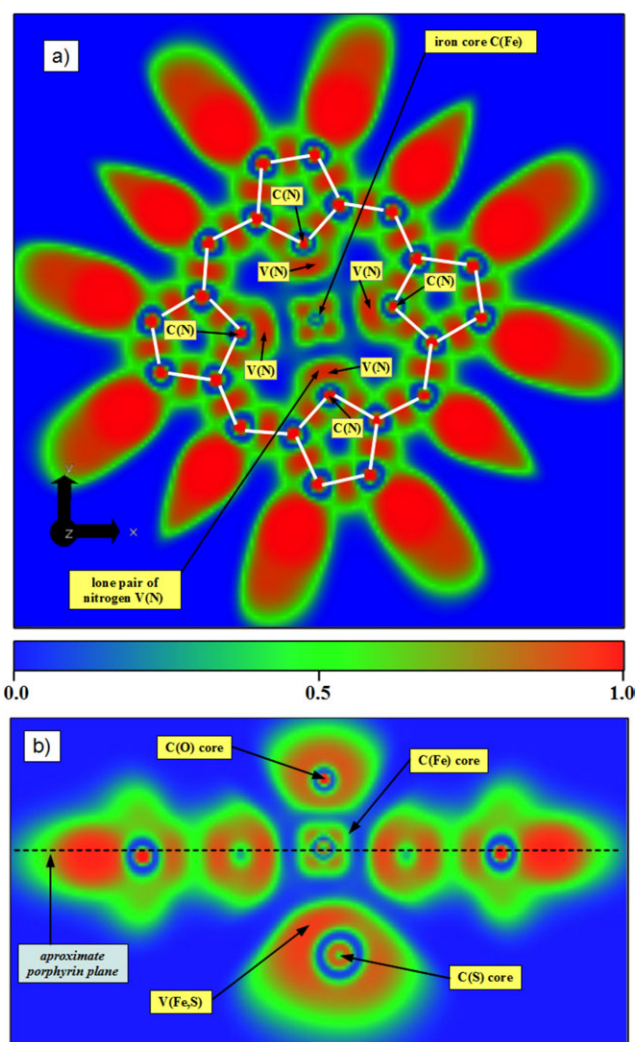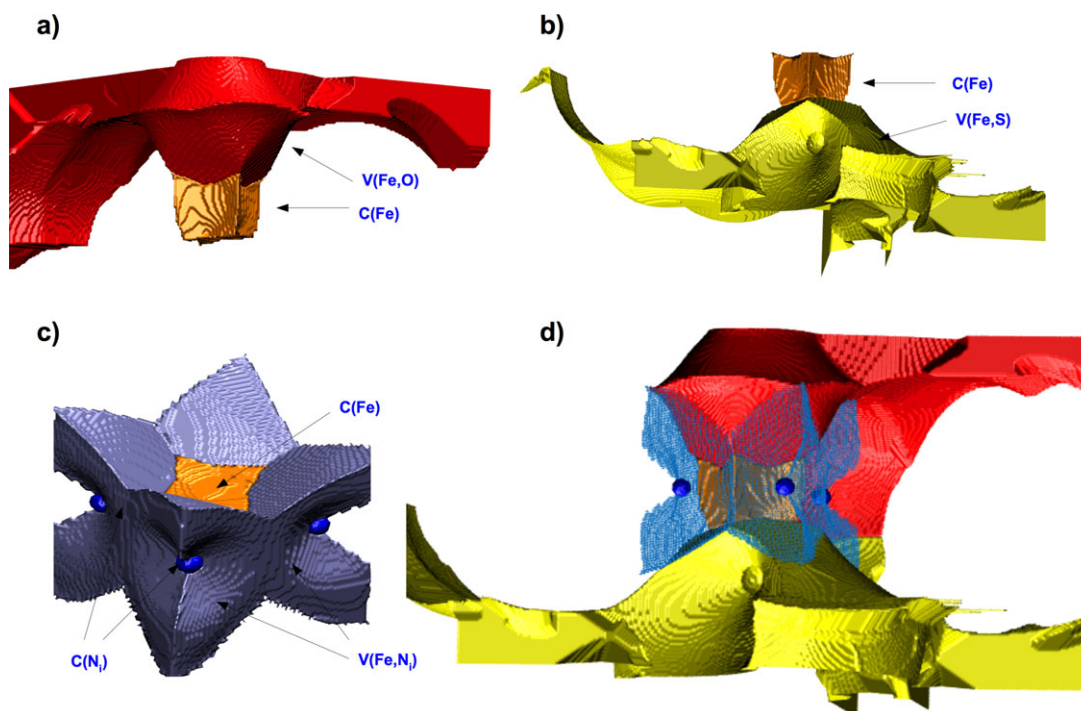

Figure 5. Two different 2D plots of the ELF function of Cpd I at the porphyrin ring plane a) and perpendicular to this plane b).

Figure 6. 3D manifolds of the iron core C(Fe) with the different valence basins of the different ligands: a) the oxygen basin V(Fe,O), b) the sulfur basin V(Fe,S), c) the four nitrogen cores C(Ni =1, 4) and basins V(Fe,Ni), and d) a combined representation of the C(Fe) core and the ligand basins.

Scheme 1) predicting the double Fe=O bond with two lone pairs on oxygen. Furthermore, is very similar to that observed for the simplest carbonyl compound H_2C=O[47–49] or in molecules with carbon monoxide ligands.[50] The positions of the $V_1(O)$ and $V_2(O)$ attractors (see Fig. 2a) suggest that the electron cloud of valence shell of the O atom is polarized to minimize the Pauli repulsion with the electron clouds associated with the $V(N)_{i=1–4}$ localization basins.

It is worth emphasizing that in the Fe···O region, where the double bond Fe=O is expected, no bonding attractor is observed (see Fig. 2b). Therefore, a clear difference between the iron–oxygen bonding and both iron–nitrogen and iron–sulfur bonding can be observed. Therefore, the covalent bond (Fe—O) or covalent-dative bond (O→Fe) between Fe and O is missing and, from the point of view of the ELF topology analysis, the nature of the binding stems mainly from $Fe^{\delta+}$···$O^{\delta-}$ electrostatic interactions. Similar results have been reported for other metal-oxygen bonds in the literature.[34,35]

The analysis of the synaptic order performed for the valence basins of the oxygen atom shows (see Fig. 6a) that they also have common surfaces with the iron core and might be classified to the disynaptic type V(Fe,O). However, this result does not testify about covalent character of the bonding since the basins (and attractors) are clearly associated with the lone pairs (see Fig. 2b). Nevertheless the analysis of the

covariance matrix of the ELF calculations reveals the presence of 0.43e localized among the iron and oxygen lone pairs (see Supporting Information Table S3). This fact could be an indicator of a large fluctuation of the electronic density between these basins, which in turns could indicate the presence of a charge-shift bond.[51]

Finally, the mean electron populations calculated for selected core and valence basins are presented in Table 3. The iron core, represented by the C(Fe) basin, contains 23.72e (M = 2, 4) and a value of the alpha spin density ($n_\alpha - n_\beta$) of 1.24e (M = 2, 4). The analysis of the spin density calculated for the η-basins between the doublet to quartet electronic states, shows different results. The values of the basin population and spin densities summed up for different fragments of the $Por^{\cdot+}$ Fe^{IV}=O(S—H) complex are also showed in Table 3. On one hand, there is a lack of spin density change for the iron core, oxygen atom, oxygen–iron bond, and the nitrogen lone pairs (represented by the $V(Fe,N)_{i=1–4}$ basins). Thus, local electronic

Table 2. Basin populations of for the hydrogen sulfide H_2S, hydrosulfide ion $[HS]^-$, hydrosulfide radical $[HS]$, and HS fragment in Cpd I (M = 2, 4); as a result of the topological analysis of electron density $\rho(r)$ and electron localization function $\eta(r)$.

Basin[a]/molecule	H_2S	$[HS]^-$	$[HS]^{\cdot}$ (M = 2)	Cpd I (M = 2)	Cpd I (M = 4)
C(S)	10.07e	10.09e	10.06e	10.08e	10.08e
$V_{i=1,2}(S)$	2.15e[b]/2.15e[b]	6.12e[b]	2.59e[b]/2.58e[b]	2.75e[b]/2.68e[c]	2.77e[b]/2.66e[c]
r[$V_{i=1,2}(S)···C(S)$]	0.99 Å[d]	0.98 Å[d]	0.99 Å[d]	0.97 Å[d]/0.95 Å[e]	0.96 Å[e]/0.96 Å[e]
$V_{i=1,2}(H,S)$	1.81e/1.82e	1.80e	1.77e	1.84e	1.83e

[a] Numbering of atoms and basins according to Figure 2. [b] Single nonbonding basin V(S). [c] Disynaptic bonding basin V(Fe,S). [d] Distance between the core attractor of sulfur C(S) and attractor of the basin $V_i(S)$. [e] Distance between the core attractor of nitrogen C(S) and bonding disynaptic attractor V(Fe,S).

Table 3. The approximate total electron populations and spin electron densities [e] calculated for different fragments of the Cpd I (M = 2, 4) using the basin populations obtained from topological analysis of ELF function.

Molecular fragment/multiplicity	M = 2		M = 4	
Electron population [e]	$n_\alpha + n_\beta$[a]	$n_\alpha - n_\beta$[b]	$n_\alpha + n_\beta$	$n_\alpha - n_\beta$
Sulfur–hydrogen bond [S—H] $^{\delta-}$ C	17.35	−0.55	17.34	0.52
(S)∪V(Fe,S)∪V(S)∪V(H,S)	$\delta = -1.35$		$\delta = -1.34$	
Iron atom [Fe]$^{\delta+}$[c]	23.72	1.24	23.72	1.18
C(Fe)	$\delta = +2.28$		$\delta = +2.28$	
Oxygen atom [O] $^{\delta-}$	8.90	0.74	8.88	0.80
C(O)∪V$_1$(O)∪V$_2$(O)	$\delta = -0.90$		$\delta = -0.88$	
Oxygen–iron bond [Fe=O]$^{\delta+}$	32.62	1.98	32.60	1.98
C(Fe)∪C(O)∪V$_1$(O)∪V$_2$(O)	$\delta = +1.38$		$\delta = +1.40$	
Nitrogen N1—N4 cores and four dative N→Fe bonds	20.68	−0.22	20.68	0.20
C(N1)∪V(Fe,N1)∪C(N2)∪V(Fe,N2)∪C(N3)	$\delta = -4.68$		$\delta = -4.68$	
∪V(Fe,N3)∪ C(N3)∪V(Fe,N4)				
Porphyrin fragment	161.44	−0.43	161.52	0.50
[C$_{20}$H$_{12}$N$_4$] $^{\delta-}$	$\delta = -1.44$		$\delta = -1.52$	

[a] Total number of electrons. [b] Spin density. [c] Net charge δ calculated regarding to formal population [Ar]3d^6 4s^2.

single attractor V(C,C)$_{i=1-20}$ in the Cpd I.

5. According to the synaptic order, the Fe—N$_{i=1-4}$ and Fe—S bonds are covalent-dative bonds but the respective localization basins are "formed" by electron density from lone pairs.

6. The nature of the bonding between Fe and O, formally double Fe=O, predicted by the ELF analysis stems mainly from electrostatic interactions, as long as no bonding attractor V(Fe,O) between the C(Fe) and C(O) core attractors is observed. Conversely, the localization indexes obtained from the covariance matrix for the iron and oxygen lone-pair basins would indicate the presence of a charge-shift bond.

structure of these fragments is not affected by the electronic state. However, the essential change of spin density is observed for the porphyrin skeleton and the sulfhydryl group (S—H) since the value of $n_\alpha - n_\beta$ difference changes from −0.43e to 0.50e and −0.55e to 0.52e, respectively, when comparing the doublet with the quartet state. This is an expected result, confirming the radicalary nature of the porphyrin ring, which leads to the different multiplicities of the Cpd I.

Conclusions

For the first time, an analysis of the electronic structure of the porphyrin-iron complex Cpd I has been performed by means of the topological analysis of the ELF and electron density. Without invoking the concept of molecular orbital, we have been able to describe the nature of the chemical bonds in real space, and depict the main differences between two spin states, doublet, and quartet (M = 2, 4). The main conclusions can be summarized as follows:

1. A difference between the doublet and quartet spin states of Cpd I is seen through different positions of the V$_1$(O) and V$_2$(O) nonbonding attractors, in respect to the bonds of the porphyrin. Although the same number of valence and core attractors with the same synaptic order are observed.

2. The change of the spin state from doublet to quartet leads to a change of the spin density mainly in the porphyrin fragment and the sulfhydryl group.

3. The delocalized network of carbon–carbon and carbon–nitrogen bonds in the porphyrin macrocycle is reflected by the point attractors V(C,C)$_{i=1-20}$ and V(C,N)$_{i=1-8}$ localized approximately in the plane of the porphyrin. Since the topological analysis of $\eta(r)$ does not show pairs of the V$_{i=1,2}$(C,C) and V$_{i=1,2}$(C,N) attractors (above and below the porphyrin plane), the topological signature for the double C=C and C=N bonds are, therefore, not observed.

4. The C=C bonds in the pyrrole anion fragments [C$_4$H$_2$N]$^-$ of the native porphyrin ring are described by the V$_{i=1,2}$(C,C) disynaptic attractors, while they are "reduced" to

[1] J. S. Lee, R. S. Obach, M. B. Fisher, Drug Metabolizing Enzymes: Cytochrome P450 and Other Enzymes in Drug Discovery and Development; FontisMedia SA; Marcel Dekker: Lausanne, Switzerland, New York,**2003**.

[2] D. R. Nelson, *Hum. Genom.* **2009**, *4,* 59.

[3] P. R. Ortiz de Montellano, Cytochrome P450 Structure, Mechanism, and Biochemistry; Kluwer Academic/Plenum Publishers: New York, Boston, MA, **2005**.

[4] J. T. Groves, Y. Watanabe, *J. Am. Chem. Soc.* **1988**, *110,* 8443.

[5] J. C. Schoneboom, H. Lin, N. Reuter, W. Thiel, S. Cohen, F. Ogliaro, S. Shaik, *J. Am. Chem. Soc.* **2002**, *124,* 8142.

[6] M. Newcomb, R. Shen, S. -Y. Choi, P. H. Toy, P. F. Hollenberg, A. D. N. Vaz, M. J. Coon, *J. Am. Chem. Soc.* **2000**, *122,* 2677.

[7] S. Shaik, D. Kumar, S. P. de Visser, *J. Am. Chem. Soc.* **2008**, *130,* 10128.

[8] M. Newcomb, R. Zhang, R. E. P. Chandrasena, J. A. Halgrimson, J. H. Horner, T. M. Makris, S. G. Sligar, *J. Am. Chem. Soc.* **2006**, *128,* 4580.

[9] H. Isobe, S. Yamanaka, M. Okumura, K. Yamaguchi, J. Shimada, *J. Phys. Chem. B* **2011**, *115,* 10730.

[10] J. Rittle, M. T. Green, *Science* **2010**, *330,* 933.

[11] B. Meunier, S. P. de Visser, S. Shaik, *Chem. Rev.* **2004**, *104,* 3947.

[12] S. Shaik, D. Kumar, S. P. de Visser, A. Altun, W. Thiel, *Chem. Rev.* **2005**, *105,* 2279.

[13] S. Shaik, S. Cohen, Y. Wang, H. Chen, D. Kumar, W. Thiel, *Chem. Rev.* **2010**, *110,* 949.

[14] M. T. Green, *J. Am. Chem. Soc.* **1999**, *121,* 7939.

[15] T. Ohta, K. Matsuura, K. Yoshizawa, I. Morishima, *J. Inorg. Biochem.* **2000**, *82,* 141.

[16] D. L. Harris, *Curr. Opin. Chem. Biol.* **2001**, *5,* 724.

[17] F. Ogliaro, S. Cohen, S. P. de Visser, S. Shaik, *J. Am. Chem. Soc.* **2000**, *122,* 12892.

[18] F. Ogliaro, S. Cohen, M. Filatov, N. Harris, S. Shaik, *Angew. Chem. Int. Ed. Engl.* **2000**, *39,* 3851.

[19] S. Shaik, S. P. de Visser, F. Ogliaro, H. Schwarz, D. Schroder, *Curr. Opin. Chem. Biol.* **2002**, *6,* 556.

[20] D. Harris, G. Loew, L. Waskell, *J. Am. Chem. Soc.* **1998**, *120,* 4308.

[21] G. H. Loew, D. L. Harris, *Chem. Rev.* **2000**, *100,* 407.

[22] D. Harris, G. Loew, L. Waskell, *J. Inorg. Biochem.* **2001**, *83,* 309.

[23] D. L. Harris, G. H. Loew, *J. Porphyr. Phthalocya.* **2001**, *5,* 334.

[24] P. Hohenberg, W. Kohn, *Phys. Rev. B* **1964**, *136,* B864.

[25] R. F. W. Bader, Atoms in Molecules: A Quantum Theory; Clarendon Press, Oxford University Press: Oxford, New York, **1990**.

[26] A. D. Becke, K. E. Edgecombe, *J. Chem. Phys.* **1990**, *92,* 5397.

[27] B. Silvi, A. Savin, *Nature* **1994**, *371,* 683.

[28] H. Chevreau, F. Fuster, B. Silvi, *Actual. Chimique,* **2001**, *3,* 15.

[29] B. Silvi, I. Fourre, M. E. Alikhani, *Monatsh. Chem.* **2005**, *136,* 855.

[30] N. O. J. Malcolm, P. L. A. Popelier, *Faraday Discuss.* **2003**, *124,* 353.

[31] P. L. A. Popelier, In Intermolecular Forces and Clusters; D. J. Wales, Ed.; Springer-Verlag, Germany, **2005**; pp. 1–56.

[32] I. V. Novozhilova, P. Coppens, J. Lee, G. B. Richter-Addo, K. A. Bagley, *J. Am. Chem. Soc.* **2006**, *128,* 2093.

[33] N. Xu, J. Yi, G. B. Richter-Addo, *Inorg. Chem.* **2010**, *49,* 6253.

[34] M. D. Michelini, N. Russo, E. Sicilia, *J. Am. Chem. Soc.* **2007**, *129,* 4229.

[35] L. Gracia, P. Gonzalez-Navarrete, M. Calatayud, J. Andres, *Catal. Today* **2008**, *139,* 214.

[36] P. J. Hay, W. R. Wadt, *J. Chem. Phys.* **1985**, *82,* 299.

[37] M. J. Frisch, G. W. Trucks, H. B. Schlegel, G. E. Scuseria, M. A. Rob, J. R. Cheeseman, J. A. Montgomery,Jr., T. Vreven, K. N. Kudin, J. C. Burant, J. M. Millam, S. S. Iyengar, J. Tomasi, V. Barone, B. Mennucci, M. Cossi, G. Scalmani, N. Rega, G. A. Petersson, H. Nakatsuji, M. Hada, M. Ehara, K. Toyota, R. Fukuda, J. Hasegawa, M. Ishida, T. Nakajima, Y. Honda, O. Kitao, H. Nakai, M. Klene, X. Li, J. E. Knox, H. P. Hratchian, J. B. Cross, V. Bakken, C. Adamo, J. Jaramillo, R. Gomperts, R. E. Stratmann, O. Yazyev, A. J. Austin, R. Cammi, C. Pomelli, J. W. Ochterski, P. Y. Ayala, K. Morokuma, G. A. Voth, P. Salvador, J. J. Dannenberg, V. G. Zakrzewski, S. Dapprich, A. D. Daniels, M. C. Strain, O. Farkas, D. K. Malick, A. D. Rabuck, K. Raghavachari, J. B. Foresman, J. V. Ortiz, Q. Cui, A. G. Baboul, S. Clifford, J. Cioslowski, B. B. Stefanov, G. Liu, A. Liashenko, P. Piskorz, I. Komaromi, R. L. Martin, D. J. Fox, T. Keith, M. A. Al-Laham, C. Y. Peng, A. Nanayakkara, M. Challacombe, P. M. W. Gill, B. Johnson, W. Chen, M. W. Wong, C. Gonzalez, J. A. Pople, I. Gaussian, Eds. Gaussian 03 program (revision d02), Wallingford, CT, **2003**.

[38] B. Silvi, *J. Mol. Struct.* **2002**, *614,* 3.

[39] M. Kohout, DGrid, Version 4.5, Radebeul, DGrid 4.5 program, **2009**.

[40] JMol program: an open-source Java viewer for chemical structures in 3D version 12.2.5, 2011.

[41] W. Humphrey, A. Dalke, K. Schulten, *J. Mol. Graphics* **1996**, *14,* 33.

[42] E. F. Pettersen, T. D. Goddard, C. C. Huang, G. S. Couch, D. M. Greenblatt, E. C. Meng, T. E. Ferrin, *J. Comput. Chem.* **2004**, *25,* 1605.

[43] K. L. Stone, R. K. Behan, M. T. Green, *Proc. Natl. Acad. Sci. USA* **2005**, *102,* 16563.

[44] B. Silvi, E. S. Kryachko, O. Tishchenko, F. Fuster, M. T. Nguyen, *Mol. Phys.* **2002**, *100,* 1659.

[45] F. Fuster, A. Sevin, B. Silvi, *J. Comput. Chem.* **2000**, *21,* 509.

[46] A. Savin, B. Silvi, F. Coionna, *Can. J. Chem.* **1996**, *74,* 1088.

[47] S. Berski, G. Gajewski, Z. Latajka, *J. Mol. Struct.* **2007**, *844,* 278.

[48] I. Fourre, B. Silvi, P. Chaquin, A. Sevin, *J. Comput. Chem.* **1999**, *20,* 897.

[49] A. Sanchez-Gonzalez, S. Melchor, J. A. Dobado, B. Silvi, *J. Andres, J. Phy. Chem. A* **2011**, *115,* 8316.

[50] J. Pilme, B. Silvi, M. E. Alikhani, *J. Phys. Chem. A* **2005**, *109,* 10028.

[51] S. Shaik, D. Danovich, B. Silvi, D. L. Lauvergnat, P. C. Hiberty, *Chem.—Eur. J.* **2005**, *11,* 6358.